Available online at www.sciencedirect.com
ScienceDirect
International Journal of Multiphase Flow 32 (2006) 1254–1268
International Journal of Multiphase Flow
www.elsevier.com/locate/ijmulflow

Experimental study on local characteristics of oil–water dispersed flow in a vertical pipe ☆

Dongjian Zhao, Liejin Guo *, Xiaowei Hu, Ximin Zhang, Xin Wang

State Key Laboratory of Multiphase Flow in Power Engineering, Xi'an Jiaotong University, Xi'an 710049, China

Received 27 November 2005; received in revised form 7 June 2006

Abstract

The local flow characteristics of oil–water dispersed flow in a vertical upward pipe were studied experimentally. The inner diameter and length of the test section are 40 mm and 3800 mm, respectively. A double-sensor conductivity probe was used to measure the local interfacial parameters, including interfacial area concentration, oil phase fraction, interfacial velocity, and oil drops Sauter mean diameter. The water flow rates varied from 0.12 m/s to 0.89 m/s, while the oil flow rates ranged from 0.024 m/s to 0.198 m/s. Typical radial profiles of interfacial area concentration, oil phase fraction, interfacial velocity, and oil drops Sauter mean diameter are presented. An interesting phenomenon is that the local and cross-section-averaged interfacial area concentrations display concave change with water flow rate under constant oil flow rate. The physical mechanism of such a variation is discussed in details.

1. Introduction

Flowing mixtures of oil and water in pipes are frequently encountered both in oil wells and pipelines of chemical and petroleum industry. The interest in the transportation of oil–water mixtures has led to a number of works in the area (Chen and Guo, 1999; Angeli and Hewitt, 2000; Liu et al., 2003), which addressed to the flow patterns, averaged holdup and pressure drop. However, with the development of more accurate and reliable CFD (computational fluid dynamic) models of two-phase flow in pipes, a physical understanding of the mechanism involved in the characteristic distribution of the deformable interface is inevitably.

The basic geometrical structure of a two-phase (either gas–liquid or liquid–liquid) flow can be characterized by the phase fraction and the interfacial area concentration. The phase fraction represents the phase distribution in two-phase flow, while the interfacial area concentration describes available area for the interfacial transfer of mass, momentum and energy. Local phase distribution mechanisms in two-phase flow, which

☆ This paper was presented in the 5th International Symposium on Multiphase Flow, Heat Mass Transfer and Energy Conversion in Xi'an, China, on 3–6 July 2005.

* Corresponding author. Tel./fax: +86 29 82668769.
E-mail address: lj-guo@mail.xjtu.edu.cn (L. Guo).

0301-9322/$ - see front matter © 2006 Elsevier Ltd. All rights reserved.
doi:10.1016/j.ijmultiphaseflow.2006.06.004

are strongly linked with the interfacial structure and motions, have been yet least understood. Simultaneously as pointed out by Crowe (2004), a situation can exist in which there is a locally different distribution of particles (including bubbles and drops) but the phase fraction is the same. Therefore, in order to characterize sufficiently the basic geometrical structure of two-phase flow, the phase fraction should be combined with the interfacial area concentrate. In addition, the two parameters are also required to close the set of two-fluid model equations. According to Ishii (2003), the interfacial transfer terms in two-fluid model were expressed as the product of the interfacial area concentration and the interfacial flux. However, because of the complicated dynamics of the interfacial structure, the treatment of the interfacial area concentration in two-fluid model is not well resolved at present. Over the past ten years, much experimental work has been done about the distribution characteristics of the local phase fraction and the local interfacial area concentration for gas–liquid two-phase flow in different channels (Kalkach-Navarro et al., 1993; Hibiki et al., 1998, 2003; Sun et al., 1999; Kim et al., 2002). These studies have provided experimental data to develop the interfacial area transport equation model in gas–liquid two-phase flow (Kocamustafaogullari and Ishii, 1995; Wu et al., 1998; Hibiki and Ishii, 2000). However, few studies have been published on the distribution characteristics of local flow parameters of the flow of two immiscible liquids.

In the past ten years, Farrar and Bruun (1996) carried out the pioneering work to measure the distribution characteristics of local flow parameters in a vertical kerosene–water pipe flow. They obtained the local oil phase fraction and the turbulence structure based on the Hot-Film technique. But because of the limited flow conditions, they observed only the uniform or wall peaked radial profiles of the local oil phase fraction. Angeli and Hewitt (2000) investigated the effect of wall material of the test section on the distribution characteristics of the oil phase fraction in horizontal oil–water flow. Recently, Lovick and Angeli (2004) further studied the size distribution of drops in dispersed liquid–liquid horizontal flows under dual continuous pattern, where both phases retained their continuity and there was entrainment in the form of drops of one phase into the other. Also under dual continuous pattern of liquid–liquid horizontal flow, Elseth et al. (2004) carried out experimental study on the local distribution of velocity, turbulence and oil phase fraction. But to our knowledge, there is currently no published data available on the distribution characteristics of the local interfacial area concentration in vertical oil–water two-phase flow.

The present experiment was designed to study the local interfacial area concentration, as well as the local oil phase fraction, interfacial velocity, and oil drops Sauter mean diameter of an oil–water upward flow in a vertical pipe. Valuable insight will be provided into the physical mechanism of local flow structure in liquid–liquid two-phase flow, which will be different from that of gas–liquid two-phase flow. In what follows, Section 2 briefly describes the experimental facility and instrumentation. Section 3 refers to the double-sensor conductivity probe methodology. In Section 4, the effect of sampling frequency of the double-sensor conductivity probe on the local flow parameters measurement is investigated firstly. Then the local distribution characteristics of interfacial area concentration, oil phase fraction, interfacial velocity, and oil drops Sauter mean diameter of oil–water two-phase flow are studied experimentally. Finally, Section 5 summarizes the conclusions.

2. Experimental system and procedure

The oil–water two-phase flow experiment was carried out using a flow facility designed and constructed at State Key Laboratory of Multiphase Flow in Power Engineering in Xi'an Jiaotong University. Fig. 1 shows schematically the experimental system and the corresponding instruments. Two fluids used were tap water and 5# white oil. The viscosity of the white oil was 4.1 mPa s at 40 °C, and the density was 824 kg/m^3 at 20 °C. The levels of solubility of water in oil and oil in water were so low that the two fluids could be totally considered as being immiscible.

The test section was a vertical round tube made of acrylic resin, with a 40 mm inner diameter and a 3800 mm length. And it was transparent to allow flow visualization. Local measurements were performed at the location of $Z/D = 75$ from the entrance of the test section, at which the flow could be nearly fully-developed. Here Z is the length between the measurement location and the entrance of the test section, while D is the inner diameter of the test section. Farrar and Bruun (1996) reviewed the development of mean velocity and phase fraction profiles in two-phase flow, and found in the literature that nearly fully-developed flow could be

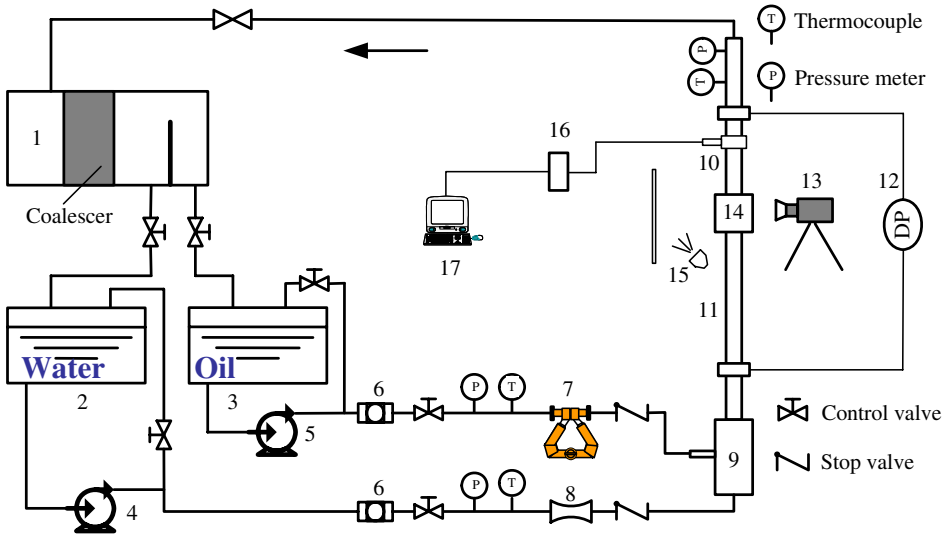

Fig. 1. Schematic diagram of experimental loop: (1) separator; (2) water tank; (3) oil tank; (4) water pump; (5) oil pump; (6) filter; (7) mass flow meter; (8) magnetic flow meter; (9) mixing chamber; (10) mechanical traverser of probe; (11) test section; (12) differential pressure transducer; (13) digital high-speed camera; (14) light compensation box; (15) light source and reflection board; (16) measurement circuit of probe; (17) PC with high-speed acquisition board inside.

obtained at $40D$ from the entrance of the test section. Therefore, $75D$ from the entrance in current work could provide fully-developed flow conditions.

During the experimentation, water and oil were supplied separately from two storage tanks, and circulated by water pump and oil pump, respectively. Before being introduced into the mixing chamber, the flow rate of oil was measured by a CMF015 Micro Motion mass flow meter with a maximum relative deviation of 0.2%, while water flow rate was measured by a magnetic flow meter with a maximum relative deviation of 0.5%. Flow rates of water and oil could both be well regulated by control valves on the feed and by pass lines. The oil and water were mixed in a mixing chamber and then the mixtures flowed upwards through the test section. Fig. 2 shows the schematic diagram of the mixing chamber. The oil drops were generated by 56 pieces of stainless steel tube located in the mixing chamber. The inner diameter of the stainless steel tube was 0.8 mm. After flowing through the test section, the mixtures of oil and water were separated through a horizontal liquid–liquid separator, and then discharged separately into the oil tank and water tank. The length and inner diameter of the horizontal liquid–liquid separator were 1.8 m and 0.6 m, respectively. In order to accelerate the separation process, a coalescer, which was made of metal wires and could promote the coalescence of the oil drops, was installed inside the separator.

Local flow parameters, including local interfacial area concentration, oil phase fraction, interfacial velocity, and oil drops Sauter mean diameter, were measured using the double-sensor conductivity probe. The details of design and application of double-sensor conductivity probe will be presented in next section. Twenty radial locations were selected across half of the test section inner diameter from $r/R = 0$ to 0.95. Here the r is the probe location from the test section center, while R is the radius of the test section. The superficial velocity of water and oil varied from 0.12 m/s to 0.89 m/s, and from 0.024 m/s to 0.198 m/s, respectively. The oil phase

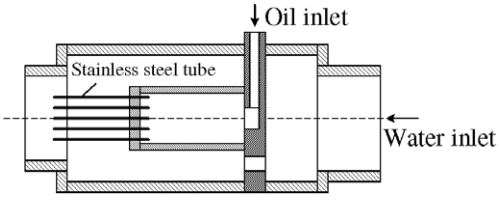

Fig. 2. Schematic diagram of the mixing chamber.

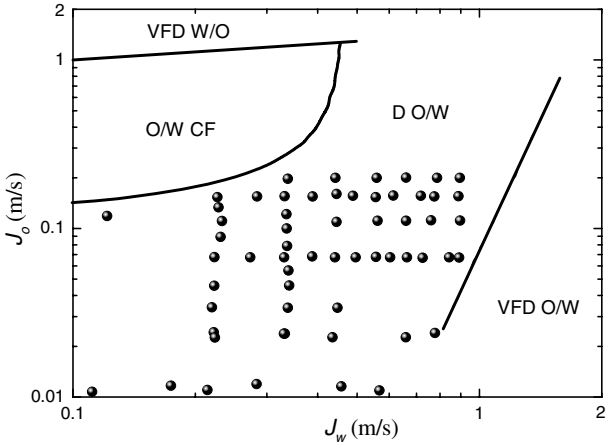

Fig. 3. Experimental conditions on oil–water two-phase flow regime map proposed by Flores (1997).

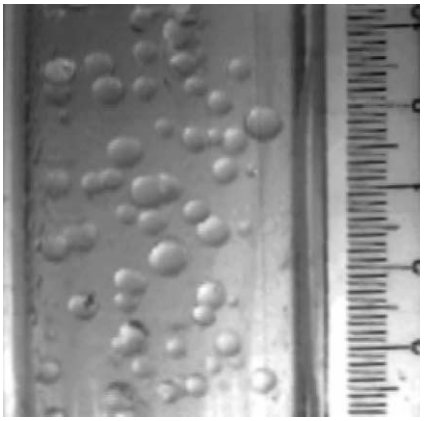

Fig. 4. Typical photographic image of the flow structure from digital high-speed camera.

fractions at test section entrance ranged from 5% to 35%. Fig. 3 presents the flow conditions in details on an oil–water two-phase flow regime map proposed by Flores (1997). In the figure, VFD O/W, DO/W and O/W CF denote very fine dispersion oil in water flow, dispersion oil in water flow, and oil in water churn flow, respectively. The oil drops dispersed in continuous water were observed in all experimental flow conditions. A typical photographic image of the flow structure from digital high-speed camera is shown in Fig. 4. The double-sensor conductivity probe method could only be used in current oil drops dispersed in water flow conditions for measuring the local interfacial area concentration.

A Keller high-frequency differential pressure transducer was used to measure the pressure drop of 1 m apart. The temperature of each fluid before mixing, and the temperature of the mixtures at outlet of the test section were measured using thermocouples. The pressures at the same locations as temperatures measurement were also measured. All data was transmitted to a personal computer and recorded using a NI PCI-6071E acquisition board with the help of NI LabView software.

3. Double-sensor probe methodology

3.1. Double-sensor probe design and measurement system

The double-sensor conductivity probe has been widely used recently to measure the local interfacial area concentration in gas–liquid two-phase flow (Hibiki et al., 1998, 2003; Sun et al., 1999; Kim et al., 2002). It

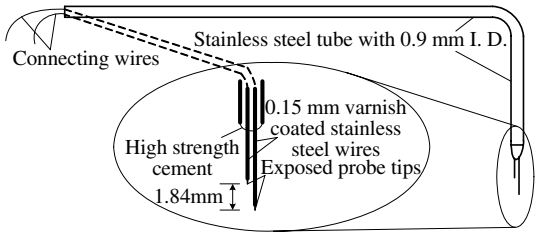

Fig. 5. Schematic diagram of the double-sensor conductivity probe.

was composed of two sensor electrodes and an external stainless steel tube, which was considered as the grounded terminal. The double-sensor conductivity probe could carry out the instantaneous measurement of the change of local electrical resistivity in two-phase flow. In an oil–water flow, the oil can be generally considered as an electrical insulator, whereas water is an electrical conductor. In order to ensure that the grounded terminal always contacted with continuous electrical conductor, experiments in present work were all carried out within the oil drops dispersed in continuous water flow regime. When one of the sensors was in contact with the water, the circuit was closed. When it was in contact with an oil drop, the circuit was open. Each sensor and the return electrode were connected to their own measuring circuit and, therefore, each sensor was used independently as a phase identifying device.

Fig. 5 shows a schematic diagram of the double-sensor conductivity probe designed in our Laboratory. The probe sensors were made of stainless steel wires with a diameter of 0.15 mm. Through chemical corrosion, each wire was acuminated to a fine needlepoint with a diameter about 0.02 mm estimated by microscope. This configuration could perfectly minimize oil drops deformation when impacting with the sensors. Then the two sensor wires were insulated with insulating varnish, keeping the tip of each stainless steel wire exposed. Both wires were inserted into a stainless steel tube with an inner diameter of 0.9 mm and with a 90° elbow. The distance between the two tips of the wires were adjusted to about 2 mm. Except the tips, both sensor wires were bounded to the stainless steel tube with high strength epoxy cement. Finally, a precise measurement of the distance between the two tips of the double-sensor conductivity probe was performed using a microscope.

The double-sensor conductivity probe measurement system was consisted of a double-sensor conductivity probe, a mechanical traverser, a measurement circuit, a digital high-speed acquisition board, and the software for signal processing. The double-sensor conductivity probe was attached to the mechanical traverser mounted on a specially designed flange, and could be moved back and forth along the radial direction of the test section. A DC electric circuit was designed to measure the variety of potential difference between the exposed tip and the grounded terminal. A high-speed NI PCI-6110E acquisition board and a personal computer were used to carry out the data sampling with the help of a control program developed under the NI LabView software environment. The maximum sampling rate of the NI PCI-6110E acquisition board was 5 MHz. The sampling frequency and the sampling time in present work are 80 kHz for each channel and 40 s, respectively. For a mixture velocity of 1.5 m/s, this sampling frequency gave 19 μm precision of local flow structure in oil–water two-phase flow. It was found that this combination provided a sufficiently large volume of data for statistical analysis. The signal was sampled and saved in a personal computer for further processing. For each set of experimental data, the local interfacial area concentration, oil phase fraction, interfacial velocity, oil drops Sauter mean diameter, and oil drops frequency can be obtained.

3.2. Signal processing

A double-sensor conductivity probe was designed to measure the variety of potential difference when the sensor electrodes were in contact with water or oil. However, due to the finite size of the sensor, the possible deformation of the oil–water interface, and the time delay needed to wet or rewet the sensor tips, the output signal from the double-sensor conductivity probe differed from an ideal two-state square-wave. A suitable signal processing technique was therefore needed to extract the required information from the raw signal. Because the absolute values of the base voltage of the signal from different experimental conditions were

possibly different, the raw signal was firstly transformed to normalized signal ranging from 0 to 1 using the following equation:

$$S_{n,i} = \frac{S_i - S_{\min}}{S_{\max} - S_{\min}} \tag{1}$$

where S_i, $S_{n,i}$, $S_{\max}$, and $S_{\min}$ denote the ith raw signal, the ith normalized signal, the maximum and the minimum raw signal, respectively. Then, a method suggested by Angeli and Hewitt (2000) was used to regenerate the ideal square-wave signal from the normalized signal. The main idea of this method was that each signal was compared with two self-adjusting threshold levels, which represented the beginning of the rise and the fall of a signal, respectively. The two threshold levels were used as triggering criterions to identify the different phases. During this procedure, the determination of the thresholds was inevitable because some oil drops signal with very low amplitude could be ignored or noises could be recognized as oil drops. Unfortunately, there was no agreement in the literature regarding setting the threshold levels. Most of the researchers determined the threshold levels by experimental observation or experience. In present work, we determined the two threshold levels through a recurrence procedure by adjusting the maximum relative deviation between the volumetric oil flow rates measured by double-sensor conductivity probe and by mass flow meter (with maximum relative deviation only 0.2%) in 3%. This procedure is summarized in Fig. 6 and is explained by the following.

Firstly, two initial threshold levels were set through experimental observation, and the normalized signal was transformed to the ideal square-wave signal by the method suggested by Angeli and Hewitt (2000). Thus, the local time-averaged oil phase fraction could be obtained from the ideal square-wave signal as

$$\alpha = \frac{1}{\Delta T}\sum_{j}^{N}(T_{\mathrm{UF}} - T_{\mathrm{UR}})_j \tag{2}$$

where ΔT, T_{UF} and T_{UR} were the total sampling time, the falling time and the rising time of the jth pulses in upstream sensor signal, respectively. The number of oil drops that hit the sensor, N, could be measured by counting the number of pulses in the upstream sensor signal.

As for the interfacial velocity, however, when oil drop velocity fluctuation was considered, the lateral motions of an oil drop could cause non-effective signal. Those included either one of the sensor tips did

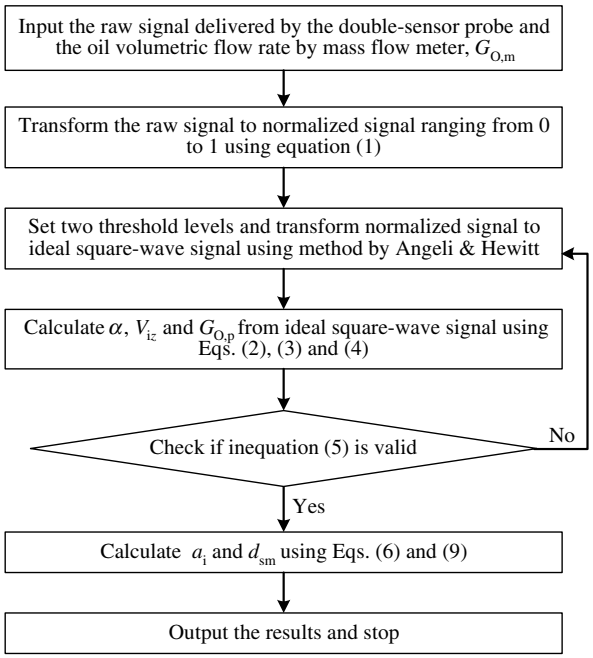

Fig. 6. Flow diagram for determination of local flow parameters from the double-sensor conductivity probe signal.

not touch the oil drop with a flat signal output, or the signal from the upstream sensor fell behind that of the downstream sensor. In order to calculate the interfacial velocity reasonably, a method suggested by Kalkach-Navarro et al. (1993) for gas–liquid bubbly flow was employed to detect the effective signal. They considered that the effective signal for interfacial velocity calculation should satisfy the following conditions: (1) the upstream sensor signal rises or falls before the downstream sensor dose; (2) the residence time of a oil drop in the upstream and downstream sensors should be comparable (typically 30%) to ensure that both sensors detect the same oil drop; (3) the time that it takes a oil drop to get from the upstream to the downstream sensor should be longer than some minimum time corresponding to the maximum possible oil drop velocity and should be shorter than the maximum time corresponding to the minimum possible oil drop velocity. From the effective signal based on above method, the local time-averaged interfacial velocity could be given as

$$V_{\mathrm{iz}} = \frac{1}{N_v}\sum_{j}^{N_v}\frac{\Delta s}{(T_{\mathrm{DR}} - T_{\mathrm{UR}})_j} \tag{3}$$

where N_v, Δs and T_{DR} were the total number of effective oil drop pulses, the distance between two tips of the sensors, and the rising time of the jth pulses in downstream sensor signal, respectively.

The oil volumetric flow rate could also be expressed as cross-section integral of the product of local oil phase fraction and local interfacial velocity in main flow direction measured by double-sensor conductivity probe

$$G_{\mathrm{O,p}} = \int_0^R 2\pi r\alpha(r)V_{\mathrm{iz}}(r)\,\mathrm{d}r \tag{4}$$

According to mass conservation, the oil volumetric flow rate obtained by double-sensor conductivity probe should be equal to the value measured by mass flow meter. Therefore, we determined if the two threshold levels set initially were reasonable by

$$|G_{\mathrm{O,p}} - G_{\mathrm{O,m}}|/G_{\mathrm{O,m}} \leqslant 0.03 \tag{5}$$

where $G_{\mathrm{O,m}}$ was the oil volumetric flow rate measured by mass flow meter. If above inequation was invalid, the two threshold levels were reset and above calculation procedure was repeated. Otherwise, the two threshold levels were reserved, and the local interfacial area concentration and local oil drops Sauter mean diameter were calculated using the following method.

Formulations for local interfacial area concentration measurement using double-sensor conductivity probe have been developed by different researchers (Kalkach-Navarro et al., 1993; Hibiki et al., 1998; Kataoka et al., 1986; Wu and Ishii, 1999). Zhao et al. (2005) compared and evaluated those formulations based on the experimental data of digital high-speed camera system in air–water bubbly two-phase flow. The results showed that the area-averaged values of local interfacial area concentration calculated using formulation proposed by Kataoka et al. (1986) agreed best with experimental data of digital high-speed camera system within a relative deviation of 12.7%. Therefore, the method proposed by Kataoka et al. (1986) was used to obtain the local interfacial area concentration in present oil–water dispersed flow.

Assuming that the oil drops were spherical, the probe passed every part of the oil drops with an equal probability, and there was no statistical relation between the interfacial velocity and the angle between the interfacial velocity and the normal vector of the oil–water interface, the local time-averaged interfacial area concentration was obtained from the harmonic mean of the interfacial velocity (Kataoka et al., 1986)

$$a_{\mathrm{i}} = 4N_t\left(\frac{\bar{1}}{|V_{\mathrm{iz}}|}\right)I(\theta) \tag{6}$$

where θ and N_t were the maximum angle between the interfacial velocity and the main flow direction, and the number of oil drops measured per unit time, respectively. On the derivation of above equation, it was also assumed that the angle between the oil drops interfacial velocity and the main flow direction was random with an equal probability within some maximum angle. Finally the function of θ was given as

$$I(\theta) = \frac{1}{1 - \cot\frac{\theta}{2}\ln\left(\cos\frac{\theta}{2}\right) - \tan\frac{\theta}{2}\ln\left(\sin\frac{\theta}{2}\right)} \tag{7}$$

The maximum angle between the interfacial velocity and the mean flow direction was determined by the statistical parameters of the interfacial velocity. Assuming that the interfacial velocity fluctuation in three directions of flow field were equal, Kataoka et al. (1986) derived the following relationship between the maximum angle and the standard deviation of oil drop velocity fluctuation in main flow direction

$$\frac{\sin 2\theta}{2\theta} = \frac{1 - \sigma_z^2/|\overline{V_{iz}}|^2}{1 + 3\sigma_z^2/|\overline{V_{iz}}|^2} \tag{8}$$

where σ_z was z component of the root mean square of the interface velocity fluctuation.

Assuming that the oil drops were spherical, based on local interfacial area concentration and local oil phase fraction, the local oil drop Satuter mean diameter was expressed as

$$d_{sm} \equiv \frac{6\alpha}{a_i} \tag{9}$$

4. Results and discussion

4.1. Effect of sampling frequency

The double-sensor conductivity probe method has become popularly used to measure the local flow parameters in two-phase flow, such as phase fraction, interfacial velocity, Sauter mean diameter, and interfacial area concentration. In present work, the effect of sampling frequency of the double-sensor conductivity probe on the local flow parameters measurement was firstly investigated. To study this influence, parts of experiments were carried out with sampling frequency as high as 320 kHz. The signal with lower sampling frequency of $320/2^n$ kHz ($n = 1, 2, 3, \ldots$) were regenerated by taking out the $2^n j$ value from the original signal, if the original signal had the form of $\{s_1, s_2, s_3, \ldots, s_j, \ldots\}$ ($j = 1, 2, 3, \ldots$).

Typically for water flow rate of 0.36 m/s and oil flow rate of 0.074 m/s, Fig. 7 shows the influence of sampling frequency of the double-sensor conductivity probe on local oil phase fraction measurement at three different radial locations across half of the diameter of the test section. In the figure, r/R is the ratio between the double-sensor conductivity probe radial location from the center of the test section, r, and the radius of the test section, R. f_S is the sampling frequency of the double-sensor conductivity probe. It can be seen that, when

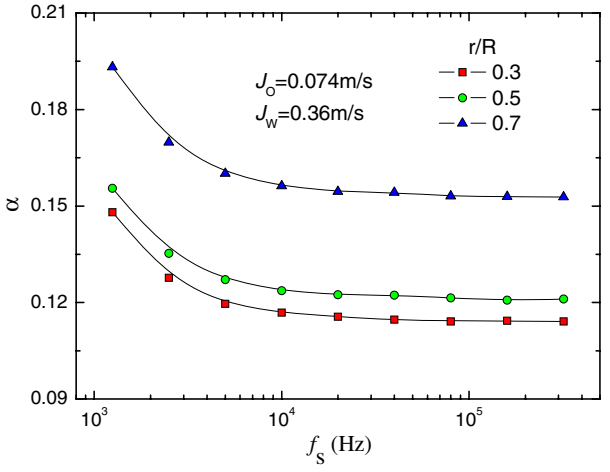

Fig. 7. Effect of the sampling frequency of double-sensor conductivity probe on local oil phase fraction measurement at three different radial locations across half of the diameter of the test section.

the sampling frequency are relatively low ($f_S < 10$ kHz), the local oil phase fraction decline sharply with an increase of sampling frequency. Then this tendency slow down gradually with further increasing sampling frequency. When the sampling frequency goes beyond 40 kHz, the local oil phase fraction basically has nothing to do with the sampling frequency. This result indicates that, lower sampling frequency may cause obvious error on local flow parameters measurement. Therefore, when using double-sensor conductivity probe method to carry out local measurement in two-phase flow, we suggest the sampling frequency should go beyond 40 kHz. This result also confirms that the sampling frequency of 80 kHz used in present work is quite reasonable.

4.2. Local phase fraction

Serizawa and Kataoka (1988) classified the phase distribution pattern in gas–liquid flow into four types. Those were the wall peak with a peak of relatively high phase fraction near the channel wall and a plateau of low phase fraction around the channel center, the intermediate peak with a broad peak of phase fraction near the channel wall and a plateau of medium phase fraction around the channel center, the core peak with a broad peak around the channel center and no peak near the channel wall, and the transition with two broad peaks around the channel wall and center. In present work of oil–water two-phase flow, we also used the definition of Serizawa and Kataoka (1988) to depict the distribution of oil phase fraction.

Based on the definition by Serizawa and Kataoka (1988), a map of local oil phase fraction distribution patterns of oil drops dispersed in water flow is illustrated in Fig. 8. We can see that when water and oil flow rates are small, the core peak characteristic distributions of oil phase fraction were observed. With increasing of oil flow rates, characteristic distributions of oil phase fraction became the transition firstly, and then the wall peak in wide flow conditions. When water and oil flow rates were great, small oil drops were finely dispersed in continuous water because of the breakup of oil drops induced by enhanced turbulent energy. And the oil phase fraction profiles became fairly uniform distributions throughout all cross-sections, without any peak both in the core and wall region of the test section.

Typical oil phase fraction profiles are presented in Fig. 9. The radial profiles of oil phase fraction for constant water flow rate of 0.33 m/s at four different oil flow rates are shown in Fig. 9a. It can be seen that for lower oil flow rate ($J_O = 0.024$ m/s), the oil phase fraction profile shows a broad core peak and a slight wall peak. With an increase of oil flow rates (typical for $J_O = 0.068$ m/s and 0.122 m/s), the oil drops tend to migrate toward the wall of the test section, and the oil phase fraction radial profiles display obvious wall peak, with a relatively flat plateau in the core of the test section. At high oil flow rate ($J_O = 0.198$ m/s), the oil phase fraction radial profile becomes intermediate peak, with a broad peak of oil phase fraction near the wall of the test section and a plateau around the center. During the experimentation, we clearly observed many oil drops

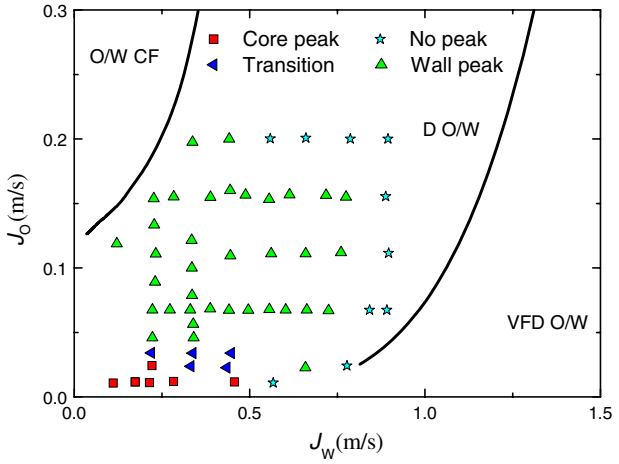

Fig. 8. Map of local oil phase fraction distribution patterns based on the definition by Serizawa and Kataoka.

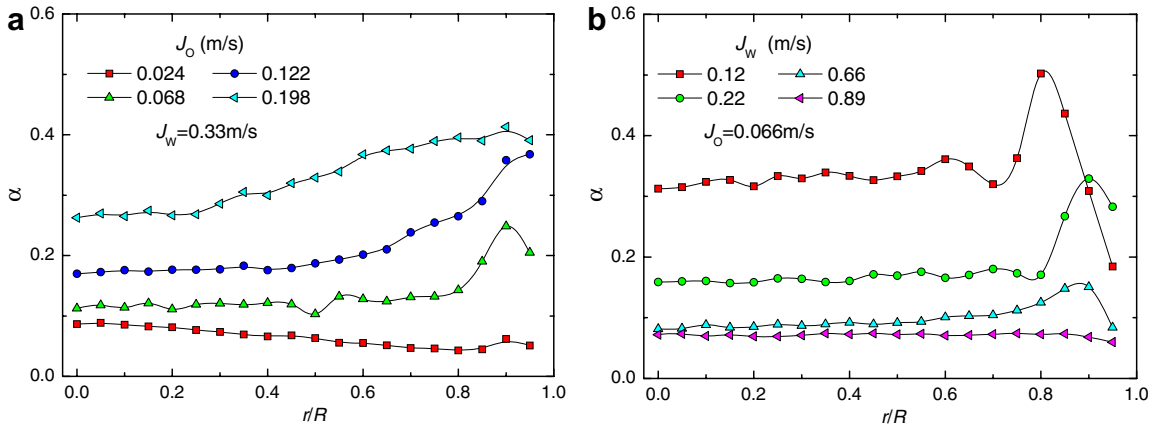

Fig. 9. Local oil phase fraction profiles at: (a) constant water flow rate ($J_W = 0.33$ m/s); (b) constant oil flow rate ($J_O = 0.066$ m/s).

went upward with rotating and rolling near very close to the wall of the test section. One reason for this could be that very close to the wall of the test section, viscous effect become important, as suggested by Liu and Bankoff (1993) in gas–liquid bubbly flow. This viscous effect finally results in increased drag on the side of the oil drops near the wall of the test section, and causes the stagnation point to be shifted away from the wall. The combination of this viscous effect and the forces perpendicular to main flow direction, such as lift force, turbulent dispersion force, may be responsible for the wall peak phenomenon. With increasing oil flow rate, the local oil phase fraction increase in general both in the core region and in the region near the wall of the test section.

The radial profiles of oil phase fraction for constant oil flow rate of 0.066 m/s at four different water flow rates are shown in Fig. 9b. We can see that for lower water flow rate (typical for $J_W = 0.12$ m/s), the oil phase fraction profile shows intermediate peak, with a broad peak of oil phase fraction near the wall of the test section and a plateau around the center. With an increase of water flow rate, typically for $J_W = 0.22$ m/s, the oil phase fraction displays wall peak clearly. The effect of further increasing water flow rate ($J_W = 0.66$ m/s) is to decrease the oil phase fraction all cross-section. This tendency can be explained that, at constant oil flow rate, increasing water flow rates raise the mixture volume of oil and water, resulting in a decrease of cross-section-averaged oil phase fraction. For water flow rate of 0.89 m/s, small oil drops are finely dispersed in continuous water because of the breakup of oil drops induced by enhanced turbulent energy. And the oil phase fraction profiles become fairly uniform distributions throughout all cross-sections, without any peak both in the core and wall region of the test section.

4.3. Local interfacial velocity and local Sauter mean diameter

Fig. 10a shows the behavior of interfacial velocity profiles, corresponding to that of oil phase fraction profiles in Fig. 9b. We can see that there is no wall peak in the interfacial velocity profiles similar to those of oil phase fraction profiles. For lower water flow rate (typically for $J_W = 0.12$ m/s), the interfacial velocity profile has a plateau around the center of the test section and decrease gradually near the wall. For water flow rates beyond 0.44 m/s, the interfacial velocity profiles have the maximum in the center of the test section and decrease gradually near the wall. With increasing water flow rate, it is seen that, as expected, the interfacial velocity increase across the test section.

Typical radial profiles of oil drops Sauter mean diameter for constant oil flow rate ($J_O = 0.066$ m/s) at different water flow rates are presented in Fig. 10b. The detected local oil drop Sauter mean diameters range from 2 to 5 mm, depending on the dynamic balance between drops breakup and coalescence in different flow conditions. The oil drop Sauter mean diameters basically display a uniform distribution along the radius of the test section. With increasing water flow rates, the oil drop Sauter mean diameters decrease obviously, because of an increase of the oil drop breakup rates induced by enhanced turbulence.

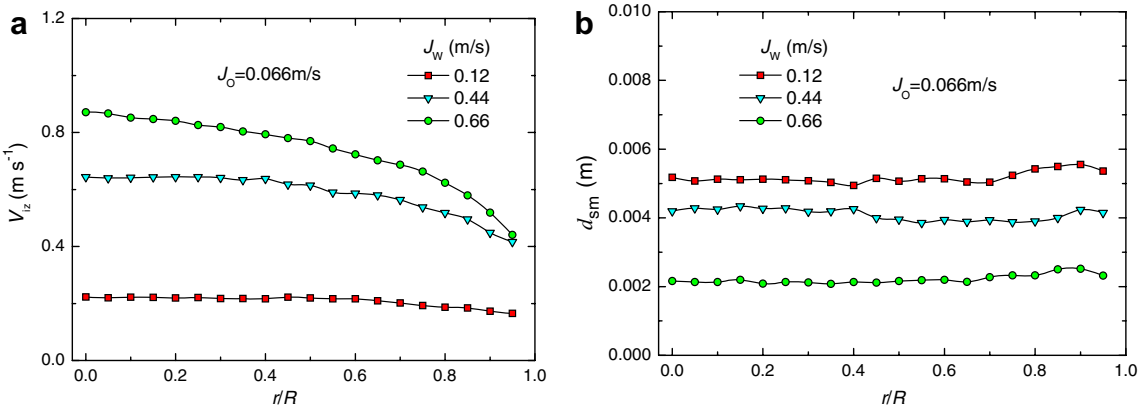

Fig. 10. Local interfacial velocity and oil drop Sauter mean diameter profiles at constant oil flow rate ($J_O = 0.066$ m/s): (a) local interfacial velocity profiles; (b) local oil drop Sauter mean diameter profiles.

4.4. Interfacial area concentration

The local interfacial area concentration profiles at constant water flow rate of 0.33 m/s are shown in Fig. 11a, corresponding to those of oil phase fraction profiles in Fig. 9a. We can see that for the oil–water dispersed flow, the interfacial area concentration profiles are quite similar to the oil phase fraction profiles. The reason for this may be that the interfacial area concentration is related directly to the oil phase fraction and oil drop Sauter mean diameter, and at the same time the oil drop Sauter mean diameter is almost uniform distribution all cross-section as shown in Fig. 10b. At lower oil flow rate (typically $J_O = 0.024$ m/s), the interfacial area concentration profile shows a slight core peak, companied with a slight wall peak. With increasing oil flow rates ($J_O = 0.068$ m/s and 0.122 m/s), the interfacial area concentration profiles display a obvious peak near the wall and are fairly flat in the core region of the test section. For higher oil flow rate ($J_O = 0.198$ m/s), the interfacial area concentration profiles become uniform distribution in the core region of the test section, with gradually decreasing near the wall region.

In Fig. 11b, the radial profiles of local interfacial area concentration at constant oil flow rate of 0.066 m/s for different water flow rates are shown. Except very high water flow rate ($J_W = 0.89$ m/s), the local interfacial area concentration profiles show obvious wall peak, with a plateau around the center of the test section. A very interesting phenomenon is that, with increasing water flow rate, the local interfacial area concentration decreases firstly for water flow rates smaller than 0.33 m/s, reach a minimum, and then increase obviously

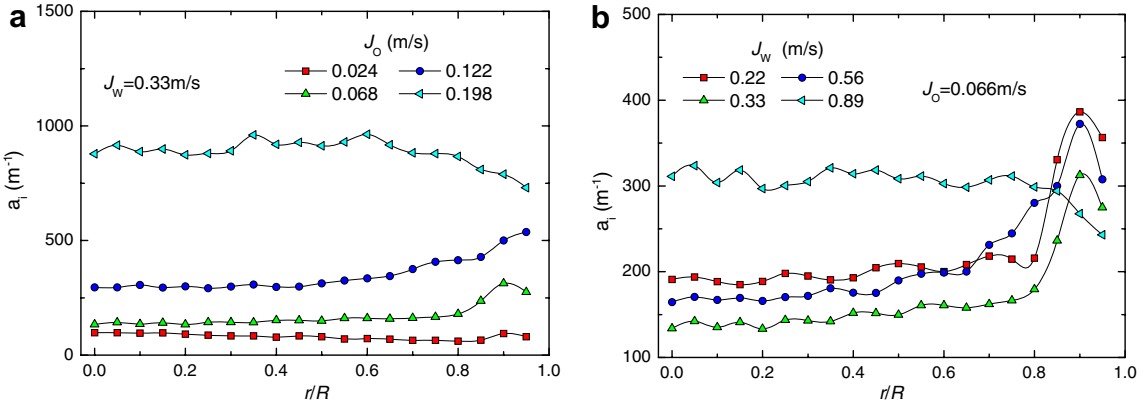

Fig. 11. Local interfacial area concentration profiles at: (a) constant water flow rate ($J_W = 0.33$ m/s); (b) constant oil flow rate ($J_O = 0.066$ m/s).

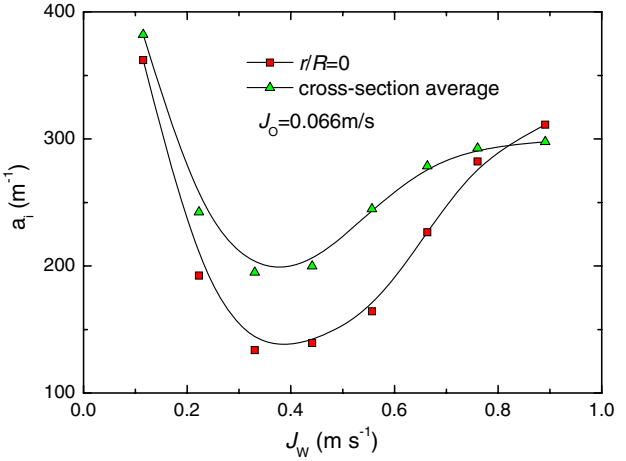

Fig. 12. Variation of cross-section-averaged and local interfacial area concentration at center-line of the test section ($r/R = 0$) with water flow rate.

when water flow rates go beyond 0.44 m/s. This implies that the oil drops breakup mechanism becomes significant above some critical flow condition.

In order to make this phenomenon clearer, the cross-section-averaged interfacial area concentration and the local interfacial area concentration at center-line of the test section ($r/R = 0$) are plotted against water flow rates in Fig. 12. The cross-section-averaged flow parameter, $\langle\phi\rangle_A$, is obtained by

$$\langle\phi\rangle_A = \frac{1}{A}\int_0^R 2\pi r\phi(r)\,\mathrm{d}r$$

where A and $\phi(r)$ denote the cross-sectional area of the test section and the local flow parameter, respectively.

We can see that both the cross-section-averaged interfacial area concentration and the local interfacial area concentration at center-line of the test section decrease firstly for water flow rates smaller than 0.33 m/s, and then increase obviously for water flow rates greater than 0.44 m/s. For lower water flow rate, the decrease of the interfacial area concentration can be explained that, at constant oil water flow rate, increasing water flow rates raise the mixture volume of oil–water two-phase flow, resulting in a decrease of cross-section-averaged oil phase fraction. At the same time, the turbulent energy has no enough force to breakup the drops into small ones. As a result, a decrease of the interfacial area concentration is obtained with increasing water flow rates. For higher water flow rates, it appears that the oil drops breakup mechanism induced by the turbulent eddy is responsible for the increase of the interfacial area concentration. With an increase of water flow rate, the large turbulence fluctuation may decrease the contact time between drops, resulting in the decrease of the oil drops coalescence rates. At the same time, the enhanced turbulence breaks up the oil drops into small ones, causing an increase of the interfacial area concentration.

Assuming that the oil drops are spherical in oil–water dispersed flow, the interfacial area concentration can be related straightway to the oil phase fraction, oil drop Sauter mean diameter and oil drop frequency. In order to clarify the tendency of the interfacial area concentration shown in Fig. 12, we also plotted the cross-section-averaged values and the local values at test section center-line of oil phase fraction, oil drop Sauter mean diameter and oil drop frequency against water flow rates in Figs. 13–15, respectively. As shown in Fig. 13, both the cross-section- averaged oil phase fraction and the local oil phase fraction at the center-line of the test section decrease sharply for water flow rates smaller than 0.33 m/s. This result seems to explain the decrease of the interfacial area concentration shown in Fig. 12. However, for water flow rates greater than about 0.44 m/s, the cross-section-averaged and local oil phase fractions decrease much slower. Another interesting result is that, for water flow rates smaller than 0.84 m/s, the cross-section-averaged oil phase fraction is greater than the local oil phase fraction at the center-line of the test section, as shown in Fig. 13. This is because the distribution pattern of the oil phase fraction profiles is wall peak, with a peak of relatively high

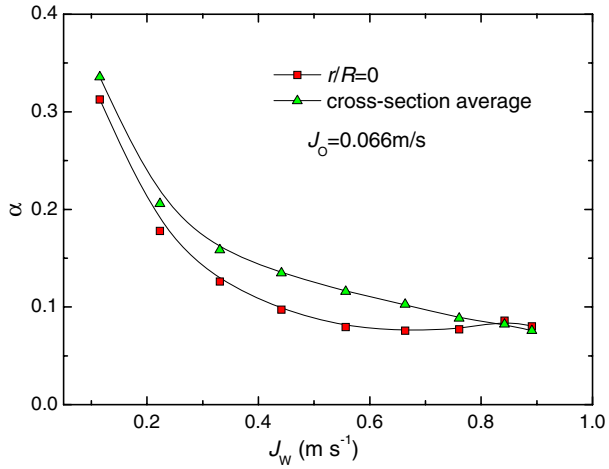

Fig. 13. Variation of cross-section-averaged and local oil phase fraction at center-line of the test section ($r/R = 0$) with water flow rate.

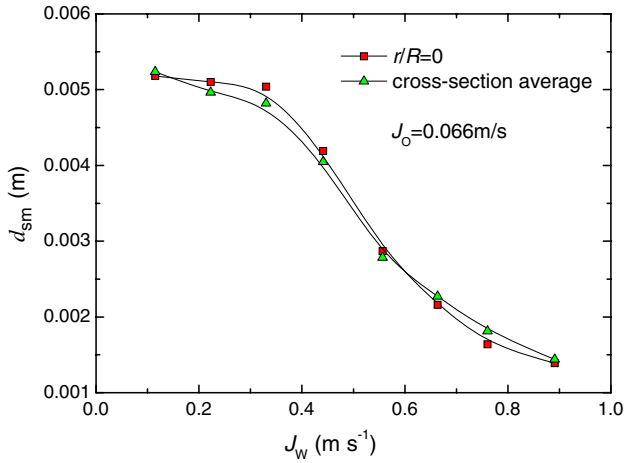

Fig. 14. Variation of cross-section-averaged and local oil drops Sauter mean diameter at center-line of the test section ($r/R = 0$) with water flow rate.

oil phase fraction near the wall of the test section and a plateau of low oil phase fraction around the center. With further increasing water flow rates, the distribution pattern of the oil phase fraction profile change from wall peak to uniform distribution, as shown in Fig. 9b. Therefore, the local oil phase fraction at the center-line of the test section becomes slightly greater than the cross-section-averaged oil phase fraction.

The cross-section-averaged oil drop Sauter mean diameter and the local value at the center-line of the test section are plotted against water flow rates in Fig. 14, corresponding to that of interfacial area concentration in Fig. 12. For water flow rates smaller than 0.33 m/s, the cross-section-averaged and local oil drop Sauter mean diameters decrease slowly. However, for water flow rates greater than 0.33 m/s, the cross-section-averaged and local oil drop Sauter mean diameters decrease dramatically from 5 mm to 1.5 mm. This implies that the oil drop breakup rates, induced by the enhanced turbulence of the oil–water dispersed flow, increase sharply. We can also draw the same conclusion from the tendency of the cross-section-averaged and the local oil drop frequencies against water flow rate, as shown in Fig. 15. Here the oil drop frequency, f_d, is defined as the number of oil drops detected by the upstream sensor per unit minute. For water flow rates smaller than 0.33 m/s, the cross-section-averaged and local oil drop frequencies change slowly, while for water flow rates greater than 0.33 m/s, the cross-section-averaged and local oil drop frequencies increase dramatically. This

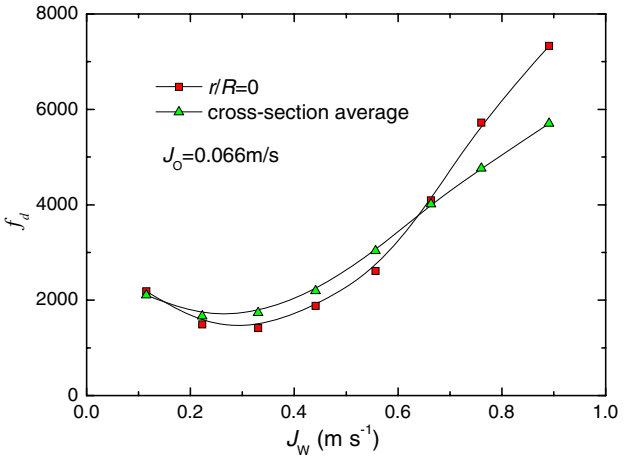

Fig. 15. Variation of cross-section-averaged and local oil drops frequency at center-line of the test section ($r/R = 0$) with water flow rate.

sharp increase of oil drop frequency also suggests the oil drops breakup phenomenon, induced by the enhanced turbulence of the oil–water two-phase, become more important. The obvious increase of oil drops breakup rates will further be responsible for the increase of the interfacial area concentration for water flow rates greater than 0.33 m/s, as shown in Fig. 12.

5. Conclusions

Using double-sensor conductivity probe method, the local distribution characteristics of interfacial area concentration, oil phase fraction, interfacial velocity, and oil drop Sauter mean diameter in oil–water dispersed flow were studied experimentally. The test section was a vertical upward pipe with an inner diameter of 40 mm and a length of 3800 mm. Firstly, we investigated experimentally the effect of the sampling frequency of the double-sensor conductivity probe on the local flow parameters measurement. The result showed that, when the sampling frequency went beyond 40 kHz, the local oil phase fraction had nearly nothing to do with the sampling frequency.

With increasing water flow rates at constant oil flow rate, the local oil phase fraction and oil drop Sauter mean diameter decreased obviously, while the interfacial velocity increased. However, the cross-section-averaged and the local interfacial area concentration decreased firstly, reached a minimum, and then increased obviously when water flow rates went beyond 0.44 m/s. This can be explained that for lower water flow rates, the decrease of the interfacial area concentration could be caused by the sharp decrease of the cross-section-averaged oil phase fraction with increasing water flow rates. With further increasing water flow rates above some critical condition, the oil drops breakup mechanism became more significant. The enhanced turbulence broke up the oil drops into small ones, resulting in the obvious increase of the interfacial area concentration. This conclusion was also supported by the tendencies of oil phase fraction, oil drop Sauter mean diameter and oil drop frequency with water flow rates.

Acknowledgements

We gratefully acknowledge the National Science Foundation of China (Contract Nos. 50536020 and 50521604).

References

Angeli, P., Hewitt, G.F., 2000. Flow structure in horizontal oil–water flow. Int. J. Multiphase Flow 26, 1117–1140.

Chen, X.J., Guo, L.J., 1999. Flow patterns and pressure drop in oil–air–water three-phase flow through helically coiled tubes. Int. J. Multiphase Flow 25, 1053–1072.

Crowe, C.T., 2004. Some comments on the needs in multiphase flows. In: Proceedings of the Fifth International Conference on Multiphase Flow, Japan.

Elseth, G., Kvandal, H., Melaaen, M.C., 2004. Measurement of velocity, turbulence and phase fraction in horizontal oil–water pipe flow. In: Proceedings of the Third International Symposium on Two-Phase Flow Modeling and Experimentation, Pisa, 22–24 September.

Farrar, B., Bruun, H.H., 1996. A computer based hot-film technique used for flow measurements in a vertical kerosene-water pipe flow. Int. J. Multiphase Flow 22, 733–751.

Flores, J.G., 1997. Oil–water flow in vertical and deviated wells. PhD Thesis, The University of Tulsa, USA.

Hibiki, T., Ishii, M., 2000. Two-group interfacial area transport equation at bubbly-to-slug flow transition. Nucl. Eng. Des. 202, 39–76.

Hibiki, T., Hogsett, H., Ishii, M., 1998. Local measurement of interfacial area, interfacial velocity and liquid turbulence in two-phase flow. Nucl. Eng. Des. 184, 287–304.

Hibiki, T., Situ, R., Mi, Y., Ishii, M., 2003. Experimental study on interfacial area transport in vertical upward bubbly two-phase flow in an annulus. Int. J. Heat Mass Transf. 46, 427–441.

Ishii, M., 2003. Outline of research for interfacial area transport phenomena in two-phase flow. Multiphase Sci. Technol. 15, 33–43.

Kalkach-Navarro, S., Lahey, R.T., Drew, D.A., Meyder, R., 1993. Interfacial area density, mean radius and number density measurements in bubbly two-phase flow. Nucl. Eng. Des. 142, 341–351.

Kataoka, I., Ishii, M., Serizawa, A., 1986. Local formulation and measurement of interfacial area concentration in two-phase flow. Int. J. Multiphase Flow 12, 505–529.

Kim, S., Sun, X.D., Ishii, M., Beus, S.G., Lincoln, F., 2002. Interfacial area transport and evaluation of source and sink terms for confined air–water bubbly flow. Nucl. Eng. Des. 219, 61–75.

Kocamustafaogullari, G., Ishii, M., 1995. Foundation of the interfacial area transport equation and its closure relations. Int. J. Heat Mass Transf. 38, 481–493.

Liu, T.J., Bankoff, S.G., 1993. Structure of air–water bubbly flow in a vertical pipe II. Void fraction, bubble velocity and bubble size distribution. Int. J. Heat Mass Transf. 36, 1061–1072.

Liu, W.H., Guo, L.J., Wu, T.J., Zhang, X.M., 2003. An experimental study on the flow characteristics of oil–water two-phase flow in horizontal straight pipes. Chin. J. Chem. Eng. 11, 491–496.

Lovick, J., Angeli, P., 2004. Droplet size and velocity profiles in liquid–liquid horizontal flows. Chem. Eng. Sci. 59, 3105–3115.

Serizawa, A., Kataoka, I., 1988. Phase distribution in two-phase flow. In: Trans. Phenomena in Multiphase Flow. Hemisphere, Washington, DC, pp. 175–225.

Sun, K.X., Zhang, M.Y., Chen, X.J., 1999. Interfacial area concentration in horizontal two-phase bubbly flow. J. Xi'an Jiaotong Univ. 33, 24–28 (in Chinese).

Wu, Q., Ishii, M., 1999. Sensitivity study on double-sensor conductivity probe for the measurement of interfacial area concentration in bubbly flow. Int. J. Multiphase Flow 25, 155–173.

Wu, Q., Kim, S., Ishii, M., Beus, S.G., 1998. One-group interfacial area transport in vertical bubbly flow. Int. J. Heat Mass Transf. 41, 1103–1112.

Zhao, D.J., Guo, L.J., Lin, C.Z., Zhang, X.M., 2005. An experimental study on local interfacial area concentration using a double-sensor probe. Int. J. Heat Mass Transf. 48, 1926–1935.